

B. TECH. PROJECT REPORT
On
**A Finite Element Study on Buckling of Thin-
Walled Steel Hollow Sections Using Geometric and
Material Nonlinearity**

BY

Ravi Jangid
Rahul Maheshwari



DISCIPLINE OF CIVIL ENGINEERING
INDIAN INSTITUTE OF TECHNOLOGY INDORE
NOVEMBER 2019

A Finite Element Study on Buckling of Thin-Walled Steel Hollow Sections Using Geometric and Material Nonlinearity

A PROJECT REPORT

Submitted in partial fulfillment of the requirements for the award of the degrees

of
BACHELOR OF TECHNOLOGY
in

CIVIL ENGINEERING

Submitted by:
Ravi Jangid
Rahul Maheshwari

Guided by:
Dr. Kaustav Bakshi
Assistant Professor



INDIAN INSTITUTE OF TECHNOLOGY INDORE
November 2019

CANDIDATE'S DECLARATION

We hereby declare that the project entitled “**A Finite Element Study on Buckling of Thin-Walled Steel Hollow Sections Using Geometric and Material Nonlinearity**” submitted in partial fulfillment for the award of the degree of Bachelor of Technology in ‘CIVIL ENGINEERING’ completed under the supervision of **Dr. Kaustav Bakshi, Assistant Professor, Discipline of Civil Engineering, IIT Indore** is an authentic work.

Further, we declare that we have not submitted this work for the award of any other degree elsewhere.

Ravi Jangid

Rahul Maheshwari

Signature and name of the student(s) with date

CERTIFICATE by BTP Guide(s)

It is certified that the above statement made by the students is correct to the best of my/our knowledge.

Signature of BTP Guide with the date and their designation

Preface

This report on “**A Finite Element Study on Buckling of Thin-Walled Steel Hollow Sections Using Geometric and Material Nonlinearity**” is prepared under the guidance of **Dr. Kaustav Bakshi**.

In this report, we have tried to determine the axial strength of thin-walled hollow sections made of mild steel by finite element model and corroborated the results with experimental data. This will help practicing civil engineers using Indian codes of Practices in choosing an adequate section for their projects

We have tried to the best of our abilities and knowledge to explain the content in a lucid manner. We have also added 3-D models, flow charts, table and figures to make it more illustrative.

Ravi Jangid, Rahul Maheshwari

B.Tech. IV Year
Discipline of Civil Engineering
IIT Indore

Acknowledgements

We wish to thank **Dr. Kaustav Bakshi** for his kind support and valuable guidance.

It is their help and support, due to which we became able to complete the design and technical report.

We also want to thank **Discipline of Civil Engineering, IIT Indore** for the funding of experimental expenses and allowing us to use the material lab equipments for our experiments.

Without their support, this report would not have been possible.

Ravi Jangid, Rahul Maheshwari

B.Tech. IV Year

Discipline of Civil Engineering

IIT Indore

Abstract

Steel having very low cost compared to the stainless steels is used in the day to day construction activities. Having more strength to the cost ratio compared to the other types steel, mild steel is preferred by practicing engineers. The present study focuses on the failure of thin-walled steel hollow tubes under axial compression which are currently being used in civil engineering projects. A finite element model considering the material and geometric nonlinearities is developed using ABAQUS package which is validated using experimental results. The experimental study is done on four circular tubes conforming IS: 1161 – 1998. The finite element model was corroborated with results obtained from the experiments. A detailed parametric study is carried out using validated finite element model on the failure of circular tubes under axial compression conforming IS: 1161 – 1998. The parametric study reports the failure loads, failure modes for varying cross-sections, length and boundary conditions. The finite element results are compared with the compressive strength values obtained using design guidelines recommended by IS: 800 – 2007. The failure loads are studied for varying length of columns so that the practicing engineers can determine the failure modes through the dimensions of the tubes.

Table of Contents

S.No.	Topic	Page No.
1	Candidate's Declaration	I
2	Certification by Guide	II
3	Preface	III
4	Acknowledgement	IV
5	Abstract	V
6	List of Figures	VII
7	List of Tables	VIII
8	Chapter 1: Introduction	1
9	Chapter 2: Finite Element Model Formulation	3
10	Chapter 3: Numerical Results and Problems	7
11	Chapter 4: Experimental Investigation	13
12	Chapter 5: Numerical Analysis of Tested Samples	19
13	Chapter 6: Results and Conclusions	23
14	Chapter 7: Future Scope of Work	29
15	References	30

List of Figures

Figure No.	Description	Page No.
1	Carbon building (Dining Hall) at IIT Indore	2
2	Shiru Café at IIT Indore	2
3	S4R Element	3
4	Structure of Proposed Finite Element Code	4
5	Stress-Strain curve	5
6	Meshed Geometry with two reference points	5
7	Mesh convergence plot	6
8	All three buckling shape modes of SHS 300 Section from linear FE code	8
9	Buckling modes of hollow sections showing axially downward displacement in mm	9
10	Comparison of buckling shapes considering Geometric Imperfections obtained from FE code	10
11	Comparison of buckling shapes obtained by Ellobody and Young [1] and FE code	10
12	Force Displacement Curves of Different Sections	12
13	Comparison of axial load values obtained from experimental, linear and nonlinear FE model	12
14	Experimental Setup	14
15	Stress- Strain curves for four sections obtained from experiments	15
16	Force- Displacement curves	17
17	Buckling shapes obtained from experiments	18
18	Comparison between force-displacement curves obtained from experiments and proposed FE code	20
19	Comparison of experimental buckling shape with proposed FE code	22
20	Comparison of Failure load vs Effective length between values obtained from FE code and IS code for Simply Supported	27
21	Comparison of Failure load vs Effective length between values obtained from FE code and IS code for Propped cantilever Supported	27
22	Comparison of Failure load vs Effective length between values obtained from FE code and IS code for Fixed Supported	27
23	Buckling shapes of ISNB 65 for three different boundary condition for four different lengths	28

List of Tables

Table No.	Description	Page No.
1	Degrees of Freedom	6
2	Comparison between buckling loads from experiments and linear finite element model	7
3	Comparison between experimental and finite element code results	10
4	Measured dimensions of column sections used for compression test	13
5	Material properties obtained from experiments	16
6	Buckling load values of tested samples from experiments	16
7	Displacement values of tested samples from experiments	16
8	Comparison between load values obtained from experiments and proposed FE code	23
9	Buckling loads for circular simply supported columns	24
10	Buckling loads for circular fixed columns	25
11	Buckling loads for circular propped cantilever columns	26

CHAPTER 1

Introduction

The thin-walled steel hollow sections are widely preferred by practicing civil engineers for superior axial and bending rigidities compared to the solid steel members of same dimensions. Such members in industrial applications may undergo failure due to instability under compressive stress. Researchers worked on buckling of thin hollow sections. Ellobody and Young [1] studied cold-formed high strength stainless steel columns compressed between fixed ends using nonlinear finite element model. The numerical results for American, Australian/New Zealand, and European standard sections were verified using experimental findings. The buckling behaviour of cold-formed high strength stainless steel stiffened and unstiffened slender square and rectangular hollow columns were studied by Ellobody [2]. Young and Rasmussen [4] studied cold-formed plain channel columns compressed between fixed and pinned ends. The nonlinear behaviour and design of pin-ended built-up cold-formed steel section battened columns were studied by Dabaon et al. [5]. The literature clearly indicates that the Indian Standard rolled steel circular hollow sections under compression is not studied by any researcher. The present study aims to fill the lacuna. The buckling behaviour of Indian Standard steel circular hollow sections are studied here using a finite element code developed using ABAQUS [3]. The geometric and material nonlinearities are considered in the proposed model.

This report describes a detailed experimental and numerical study of mild steel circular hollow sections under compressive loading. The experimental procedure was set up, and the experiments have been conducted to validate the proposed finite element model. The grade of mild steel on which the experiments performed was equivalent to YSt 300.

The present report details about the testing of concentrically loaded columns. It is followed by a detailed numerical finite element analysis, where the model is validated against the experiments performed. Upon the validation of the finite element model, a series of parametric studies is carried out using a different combination of boundary conditions and lengths of columns and are shown in the report.

Figure 1 shows the use of mild steel circular pipes as columns in building at IIT Indore to support the overhanging roof. Similarly, Figure 2 shows the mild steel square and rectangular hollow sections to enhance the aesthetics of Shiru Café at IIT Indore.

Mild steel pipes used as columns to support the overhanging roof

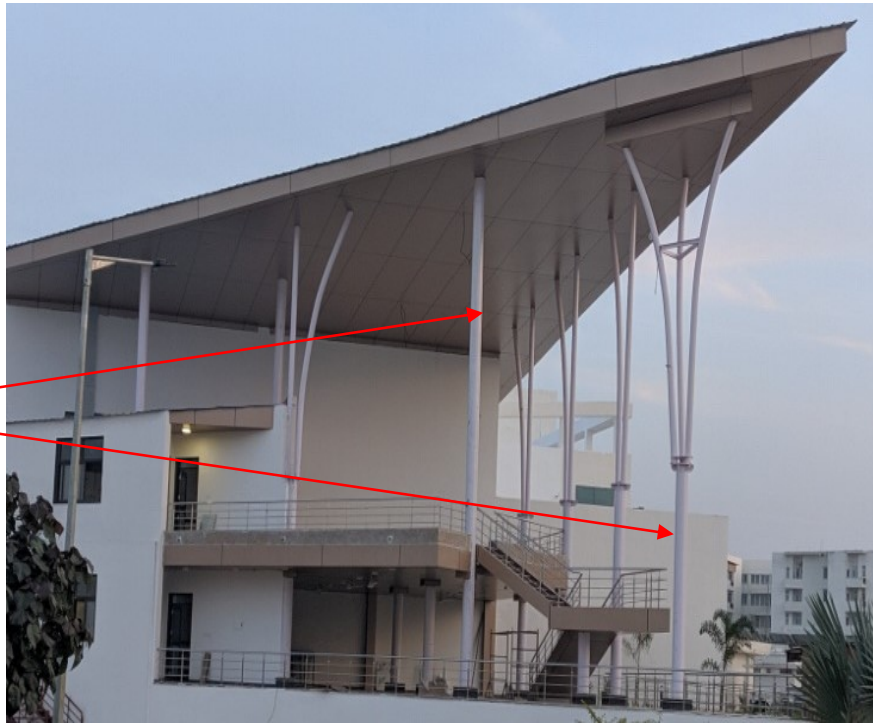


Figure 1: Carbon building (Dining Hall) at IIT Indore

Square steel pipes used for aesthetic purpose



Figure 2: Shiru Café at IIT Indore

CHAPTER 2

Finite Element Model Formulation

The finite element model has been developed using a commercial finite element package ABAQUS (2017) [3]. A four-node doubly curved shell element with reduced integration, also known as S4R, is used in the present study Figure3. A linear interpolation function is used as a shape function. Thickness to the shell element is assigned using section assignment facility available in ABAQUS [3]. First, a linear eigenvalue is also well known as Euler buckling analysis has been done by using *BUCKLE function available in ABAQUS. The analysis predicted a buckling mode of the hollow section. Then the buckled shapes are used to provide imperfection to ideal hollow section using *IMPERFECTION function. To determine the amplitude of geometric imperfection, an imperfection sensitivity study is done by taking three different amplitudes namely $t/10$, $t/100$, $L/1500$; here 't' is the thickness of the section and 'L' is the length of the column. Geometric nonlinearity is applied by using *NLGEOM in ABAQUS. No residual stress is considered as it has a negligible effect on the ultimate strength [4]. External load is applied using *RICKS method available in ABAQUS library following an increment of 0.01%.



Figure 3: S4R Element

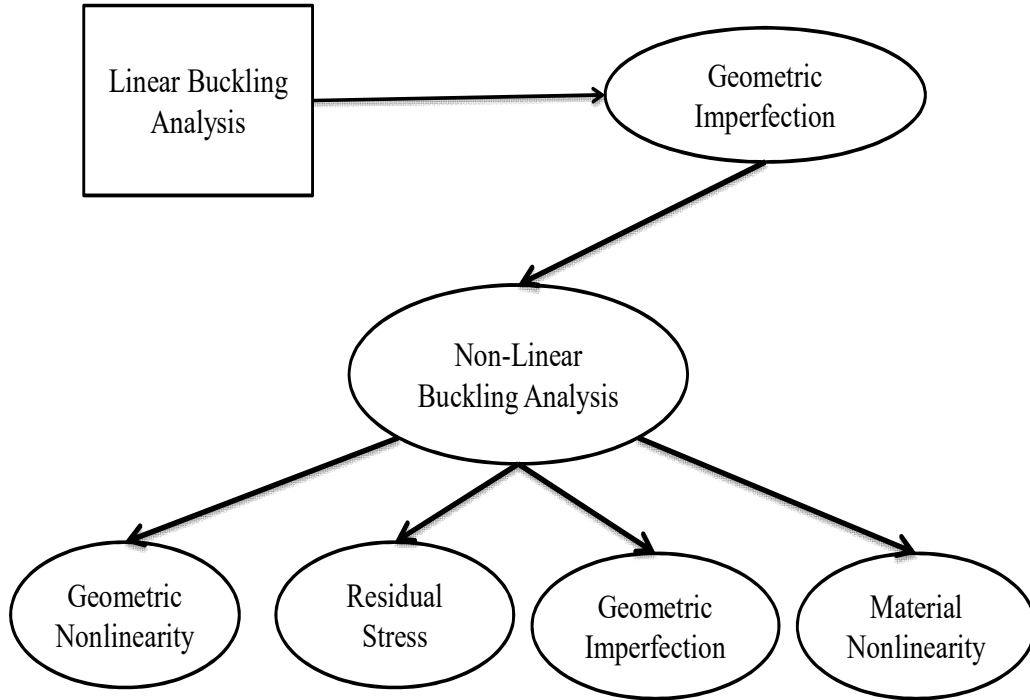


Figure 4: Structure of Proposed Finite Element Code

2.1 Material Properties

Firstly, to validate the finite element model, the high strength stainless steel is used as in used by Ellobody and Young [1]. The Origin Lab [6] tool is used to extract the experimental material data of Ellobody and Young [1]. The commercial finite element program ABAQUS uses true stress and true plastic strain data, so the data is converted accordingly using the following equations.

$$\sigma_{\text{true}} = \sigma(1 + \epsilon) \quad (1)$$

$$\epsilon_{\text{true}}^{\text{pl}} = \ln(1 + \epsilon) - \frac{\sigma_{\text{true}}}{E} \quad (2)$$

where,

E = Young's modulus from the stress-strain curve

σ_{true} = True stress developed in the material

σ = Engineering stress in the material

ϵ = Strain developed in the material

$\epsilon_{\text{true}}^{\text{pl}}$ = True plastic strain in the material

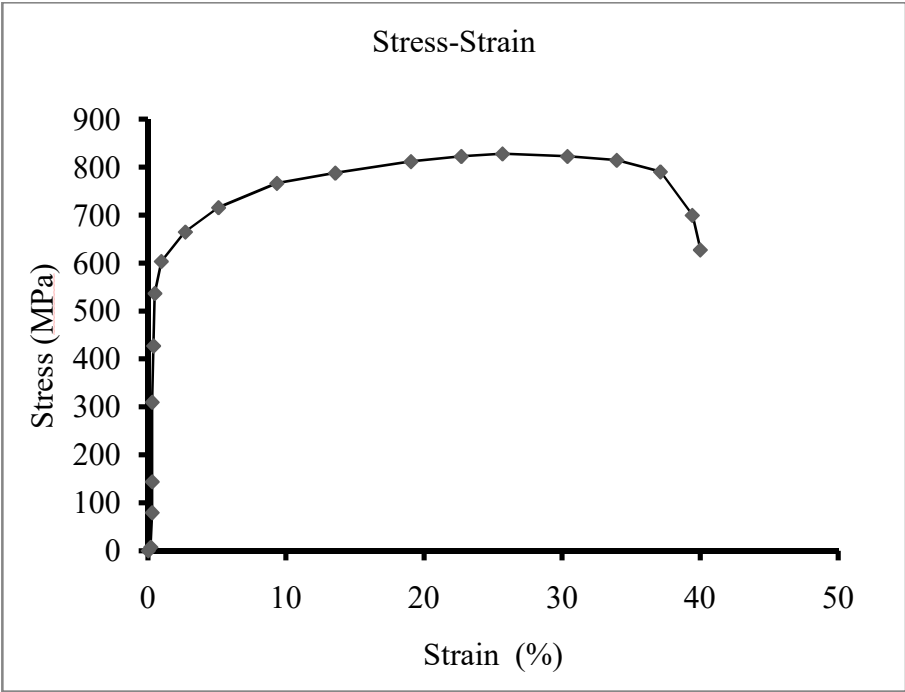


Figure 5: stress-strain curve

2.2 Boundary Conditions

The boundary condition for the present study is taken in such a way that all the degrees of freedom of both ends are fixed except degree freedom in axial direction at which the load is applied. To apply the boundary conditions and load, two reference points at the center upper and lower ends are selected, and all the perimeter nodes are associated to these reference points. The following figure and table show the degrees of freedom and their restrictions.

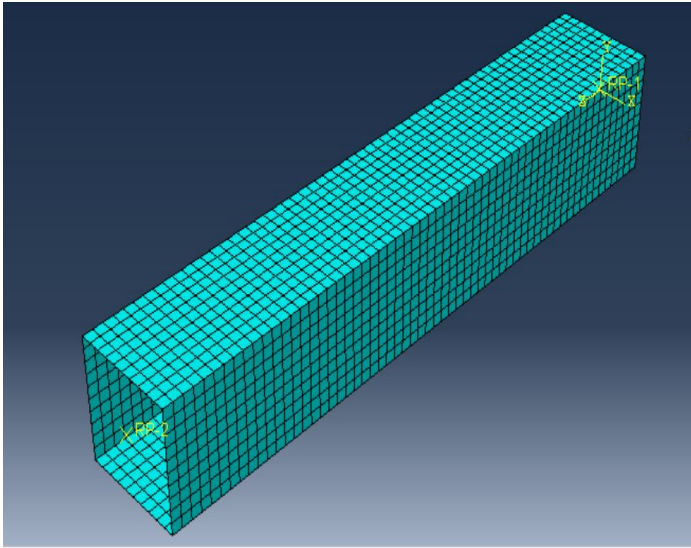


Figure 6: Meshed Geometry with two reference points

Table 1: Degrees of Freedom

DOF	R.P. 1	R.P. 2
X	0	0
Y	0	0
Z	0	1

Where '0' means restrained and '1' means free

2.3 Meshing

To determine the optimum size of mesh, a mesh convergence study is performed using linear buckling analysis. A square hollow section of length 300 mm and cross-sectional dimensions 50×50 mm with a thickness of 1.5 mm is used. Initially, a mesh size of 15 mm is taken and then mesh size is reduced up to 1.5 mm. Axial load is obtained corresponding to each mesh size and axial load plotted against the mesh size Figure7. It can be inferred from the plot that a mesh size 1.5×1.5 mm gives sufficiently accurate results without taking much computational time.

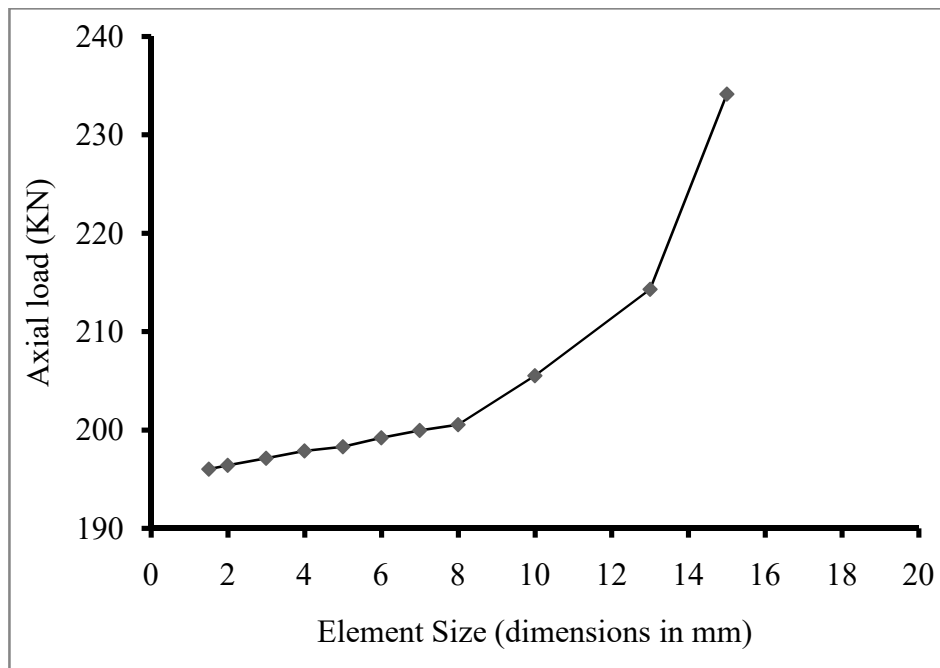


Figure 7: Mesh convergence plot

CHAPTER 3

Numerical Problems and Results

3.1 Linear Finite Element Model

To corroborate the finite element model, the experimental data provided by Ellobody and Young [1] is used. First, the buckling of sections is obtained linear finite element model, and three buckling mode shapes are extracted from the model and shown in Figure 8. The results obtained from the finite element model and experimental results are shown below in Table 2.

Table 2- Comparison between buckling loads from experiments and linear finite element model

Specimen	Section	D/t	Buckling Load (KN)	P _{Experimental} (KN)
SHS 300	50×50×1.5	33.33	195.22	175.7
SHS 650	50×50×1.5	33.33	191.43	181.0
SHS 1000	50×50×1.5	33.33	189.72	175.1
SHS 1500	50×50×1.5	33.33	182.75	156.8

NOTE: SHS 300 refers to square hollow section with a length of 300 mm

As the results clearly show that the linear finite element model is overestimating the buckling load because the linear finite element model does not account for different nonlinearities present in the material. That makes this model highly ideal without considering any imperfection in a structure like columns being out of straightness. So to overcome this situation, we need a highly nonlinear model which can replicate the real-life scenario and can predict accurate buckling loads values more close to the experimental ones.

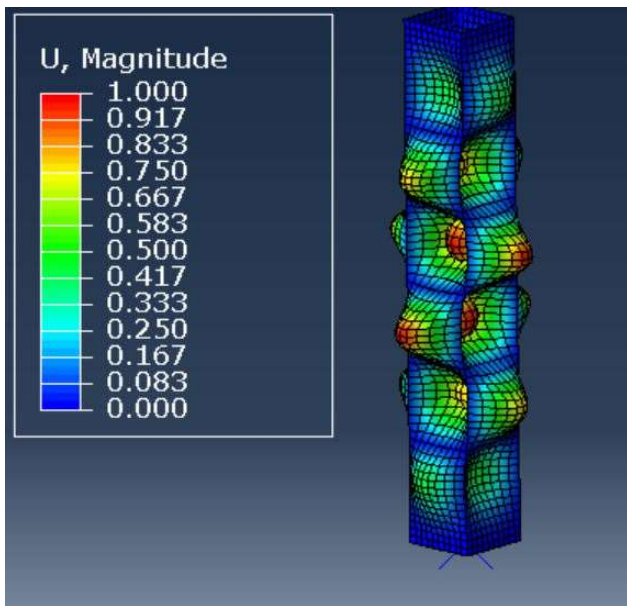


Figure 8(a): Mode 1

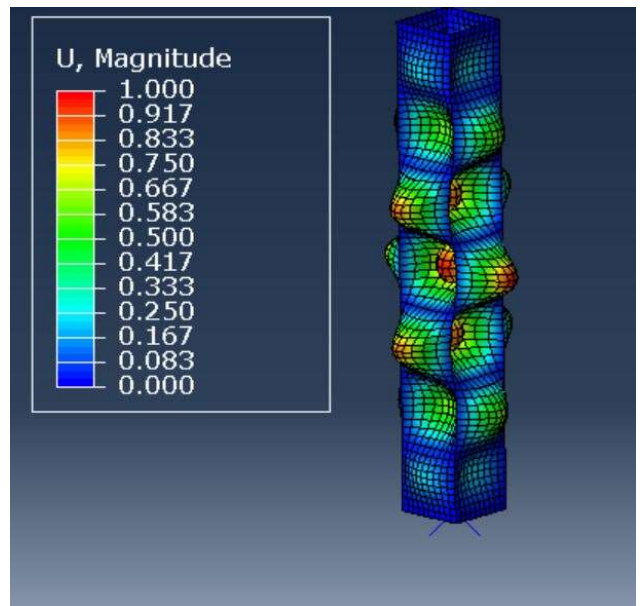


Figure 8(a): Mode 2

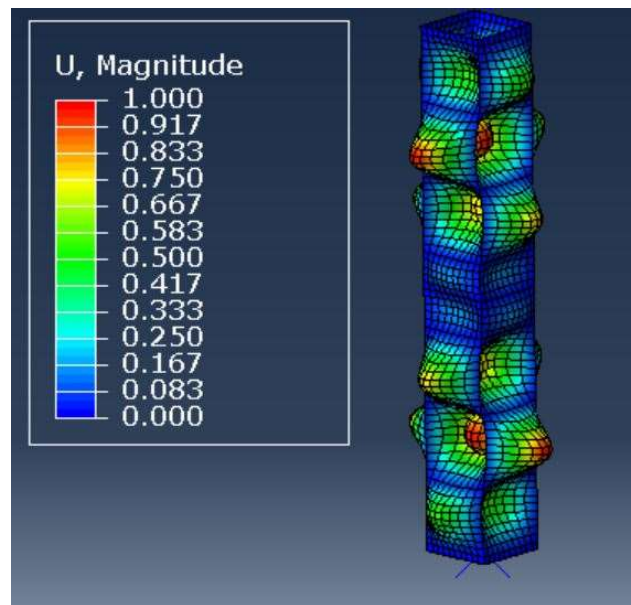


Figure 8(c): Mode 3

Figure 8: All three buckling shape modes of SHS 300 Section from linear FE code

3.2 Nonlinear Finite Element Model

The correctness of the proposed nonlinear code is confirmed by comparing the recommended buckling loads with the experimental outputs reported by Ellobody and Young [1]. The comparison is furnished in Table 2. The buckling loads and failure modes predicted by the proposed code show a very good agreement with the values reported by Ellobody and Young [1] which confirm the correctness of the proposed FE code. The nomenclature SHS 300 depicts a square hollow section 300 mm long. The SHS 650 and SHS 1500 are typically selected for further buckling study. The buckling modes showing axial compression for these two columns are shown in Figure 9. The figure shows that the maximum axial downward displacement is noted at the top of the column. The SHS 650 shows maximum lateral deformation at the mid-length. But such behaviour for the longer one, SHS 1500, is noted near to the bottom of the column. The greater geometric imperfection for the longer column may be attributed for such observation.

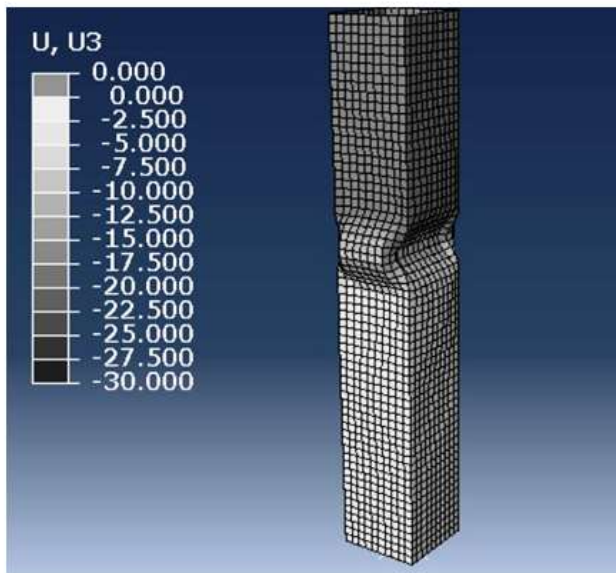


Figure 9(a): Axial displacement of SHS 650

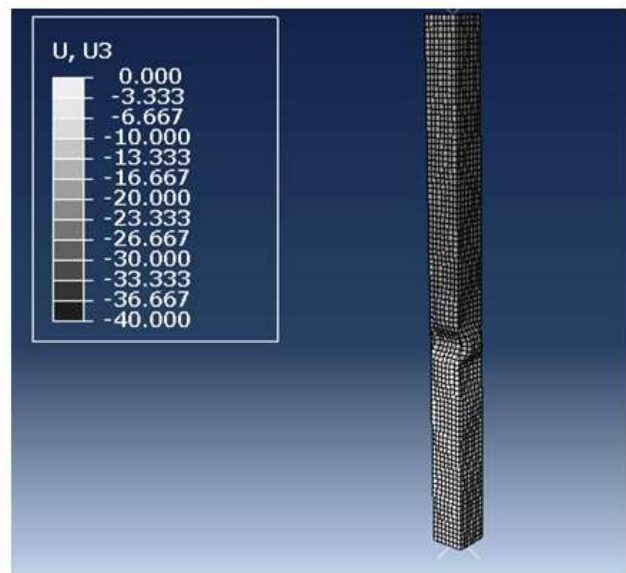


Figure 9(b): Axial displacement of SHS 1500

Figure 9: Buckling modes of hollow sections showing axially downward displacement in ‘mm’

Figure 10 shows a comparison between the two buckling shapes. Figure 10(a) shows buckling shape of SHS 300 section when the geometric imperfections are excluded from the model whereas Figure 10(b) shows the shape when geometric imperfections are included in the finite element model. From these two shapes, the conclusion can be drawn that when geometric imperfections are included in the finite element model, it gives more realistic results compared to the model without geometric imperfections.

Table 3: Comparison between experimental and finite element code results

Specimen	Section	D/t	$P_{\text{Experimental}}$ (KN) [1]	Failure Mode [1]	P_{FE} (Proposed code)	Failure Mode (Proposed code)
SHS 300	50×50×1.5	33.33	175.7	L	171.8	L
SHS 650	50×50×1.5	33.33	181.0	L	168.9	L
SHS 1000	50×50×1.5	33.33	175.1	L	164.4	L
SHS 1500	50×50×1.5	33.33	156.8	L	158.4	L

Proof Stress = 707 MPa, Ultimate tensile Stress = 827 MPa, Elongation at fracture = 29%

‘L’ refers to the buckling failure of the square hollow section

‘ $P_{\text{Experimental}}$ ’ and ‘ P_{FE} ’ refer to experimental buckling load and buckling load from finite element

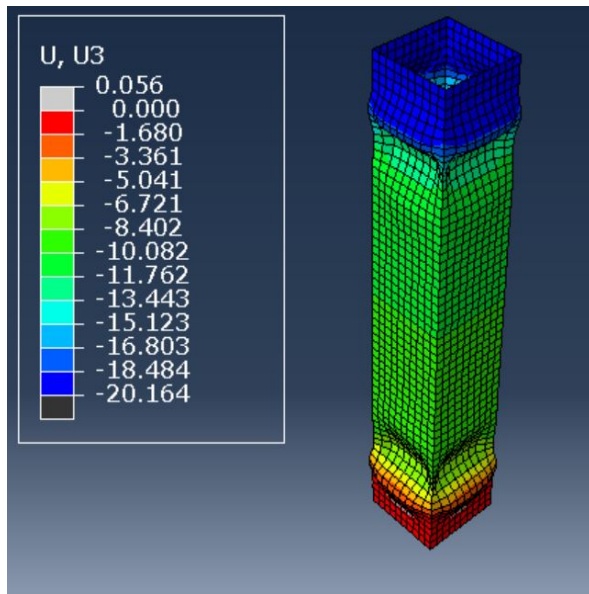


Figure 10(a): Without Imperfections

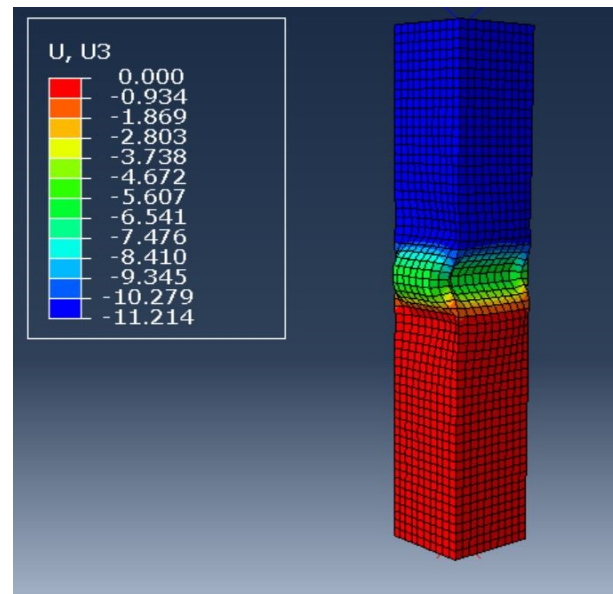


Figure 10(b): With Imperfections

Figure 10: Comparison of buckling shapes considering Geometric Imperfections obtained from FE code

Figure 11 shows that the buckling shape extracted from finite element model using geometric imperfection and buckling shape obtained by Ellobody and Young [1] from experiments show similar deflection pattern along the length.

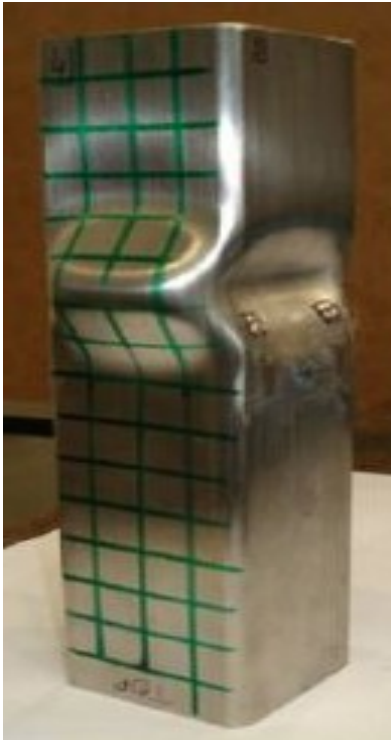


Figure 11(a): Experimental Buckling Shape

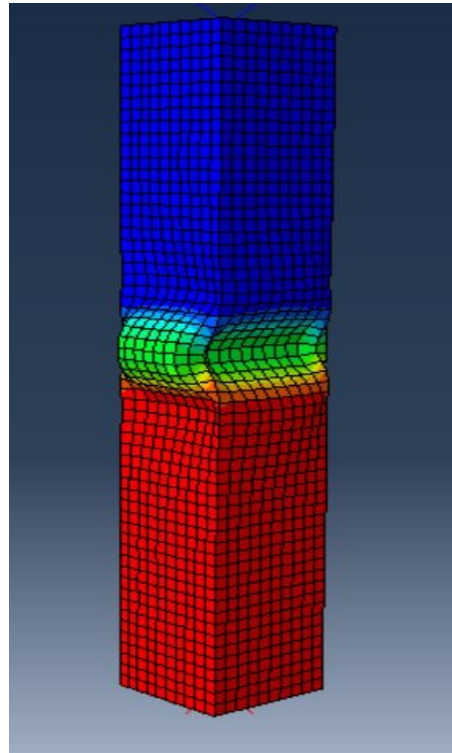


Figure 11(b): FE Buckling Shape

Figure 11: Comparison of buckling shapes obtained by Elloabody and Young [1] and FE code

Force displacement curves which show the change in stiffness of columns as load progresses incrementally are shown below for four sections obtained from the finite element model are shown in Figure 12.

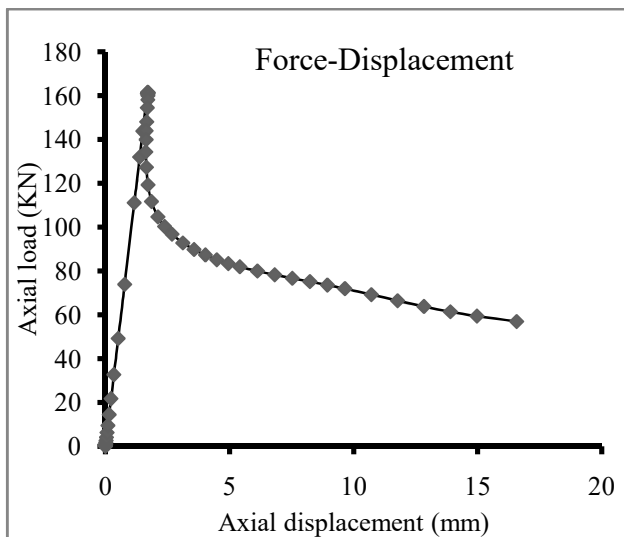


Figure 12(a): SHS 300

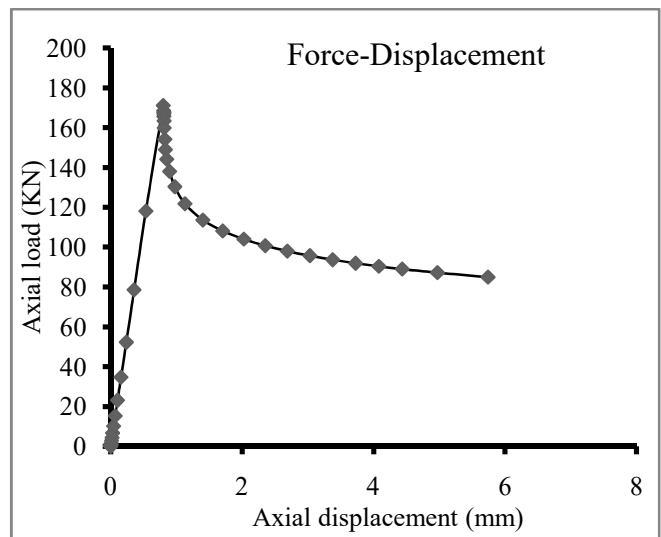


Figure 12(b): SHS 650

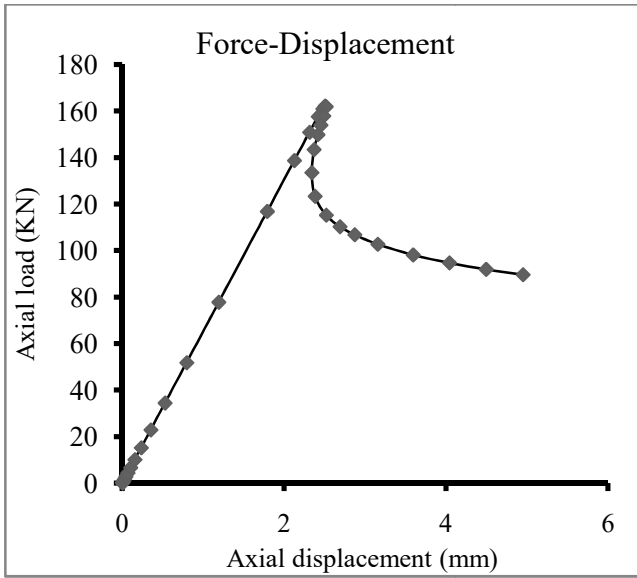


Figure 12(c): SHS 1000

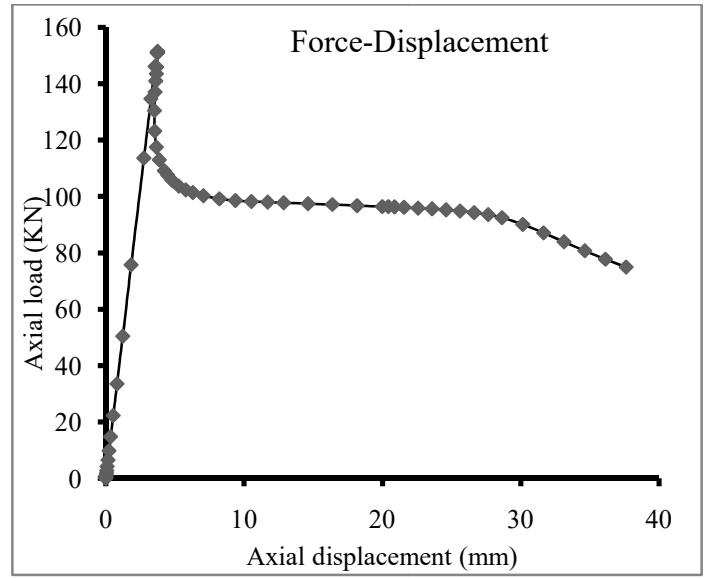


Figure 12(c): SHS 1500

Figure 12: Force Displacement Curves of Different Sections

The axial load obtained from linear and nonlinear finite element analysis and experimental results are compared in the bar diagram below. It can be inferred from the below diagram that axial load values obtained from the non-linear finite element analysis are closer to the experimental ones. So one can use proposed finite element code to determine accurate buckling loads as well as buckling shapes.

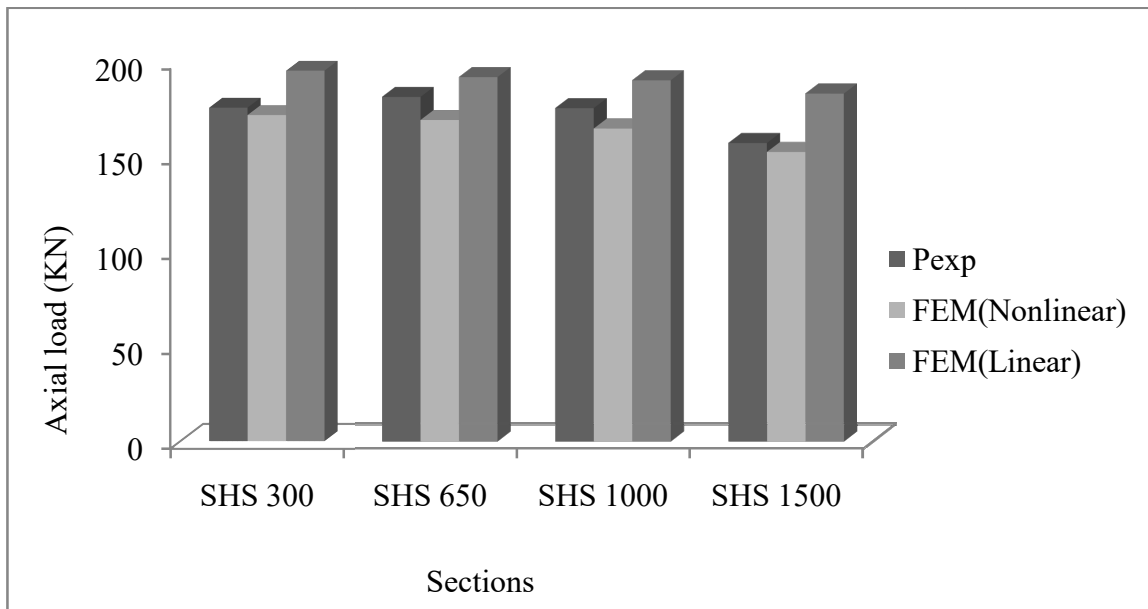


Figure 13: Comparison of axial load values obtained from experimental, linear and nonlinear FE model

CHAPTER 4

Experimental Validation

For the testing purpose, four sections are chosen from Indian codes of practice IS: 1161 (1998) and the measured dimensions are listed in Table 4 below. Length of columns was chosen in such a way that it becomes approximately four times the cross-sectional dimension of the heaviest section among all so that there can be a significant effect of overall and local buckling and yet short enough to resist flexure buckling. All the dimensions were measured with the help of the digital Vernier caliper with utmost precision. In the collection of testing samples, only the medium sections were chosen since they are most frequently used and readily available in the market.

Table 4: Measured dimensions of column sections used for compression test

S. NO.	Section	Length(mm)	Diameter (mm)	Thickness (mm)
1	ISNB 40	506	48.11	4
2	ISNB 50	503	60.39	4.65
3	ISNB 65	505	76.34	5.72
4	ISNB 80	510	89	5.95

Note: ISNB 40 represents circular hollow section with nominal bore hole of 40 mm diameter

The experimental setup consists of a Universal Testing Machine (UTM) with a computer connected to it and having a maximum capacity of 500 KN. To provide a fixed support, two metal plates are used having a thickness of 12mm each. These metal plates are made of steel which has higher yield strength than the one used in testing samples to avoid the possibility of pipes damaging the base of UTM itself. The software DATASCAN is used to record the data at an interval of one second.

Figure 14 shows the picture of the experimental setup used for compression testing. Pipe sections were placed in such a manner that the center of pipe coincides with the center of the plate. Both ends of the pipe were made flat to avoid any error in experimental load values and displacement. All the experiments were performed under the same environmental and same end boundary conditions. All the experimental obtained from the DATASCAN software is extracted and processed using Origin Lab [6]. All the samples procured from the vendor were having small patches of rust on them which will have a significant effect on the strength of the column. To avoid that, efforts were made to remove the rust using a wire brush and clean cloth.

Axial displacement was measured by the machine itself and values were extracted. But the machine does not have any setup to measure the lateral displacement. So lateral displacements were measured using plumb bob which was suspended freely from the one end of pipe and displacement was recorded using the digital Vernier caliper.

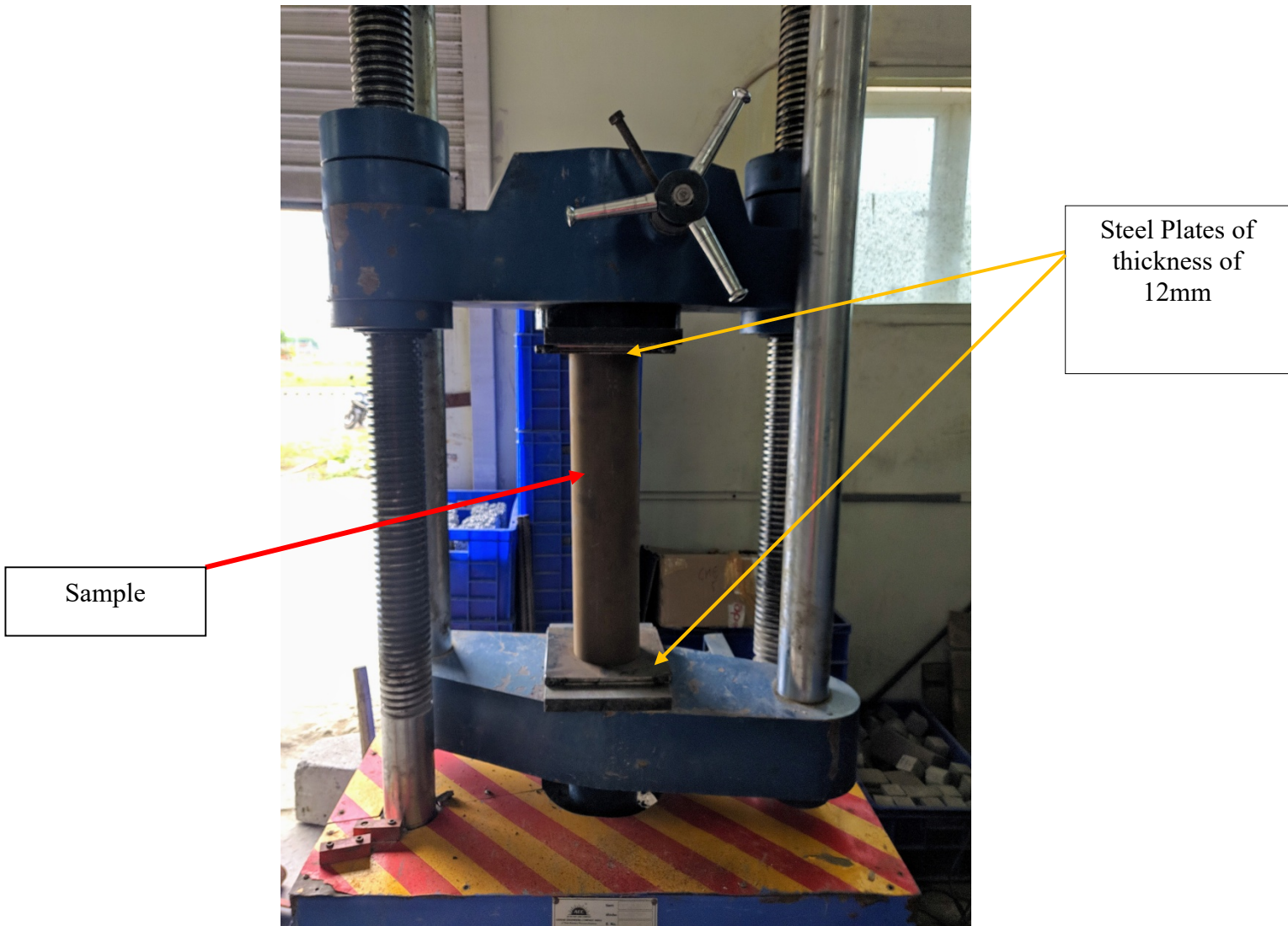


Figure14: Experimental Setup

4.1 Experimental Data

The material response curves for all four sections obtained from the experiments are shown below in Figure 15. Since the UTM does not give stress–strain curve directly, the force displacement curves have been converted into the stress–strain curves using following formulae.

$$\text{Stress} = \frac{\text{Axial Force}}{\text{Area}} \quad (3)$$

$$\text{Strain} = \frac{\text{Axial Displacement}}{\text{Total length of column}} \quad (4)$$

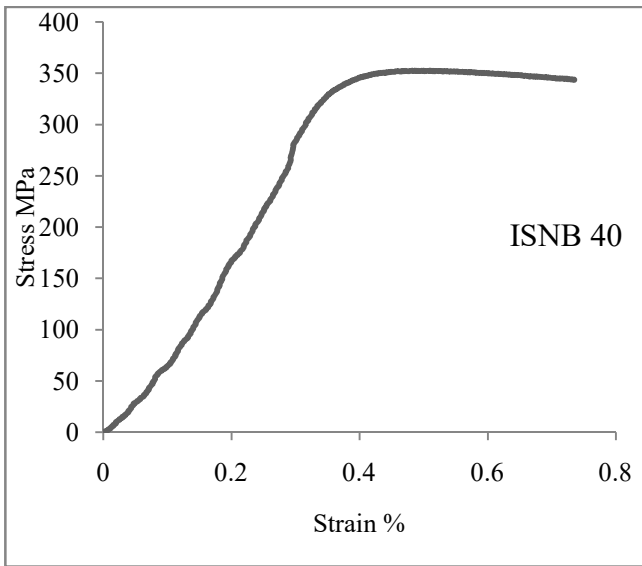


Figure 15(a): ISNB 40

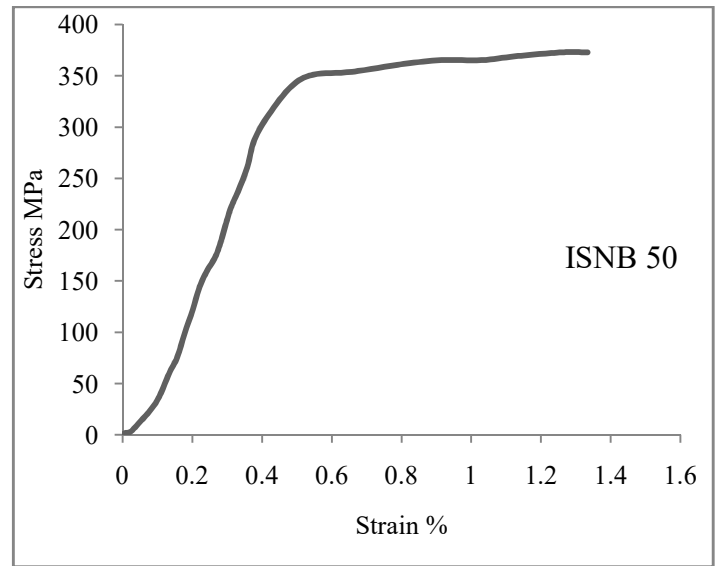


Figure 15(b): ISNB 50

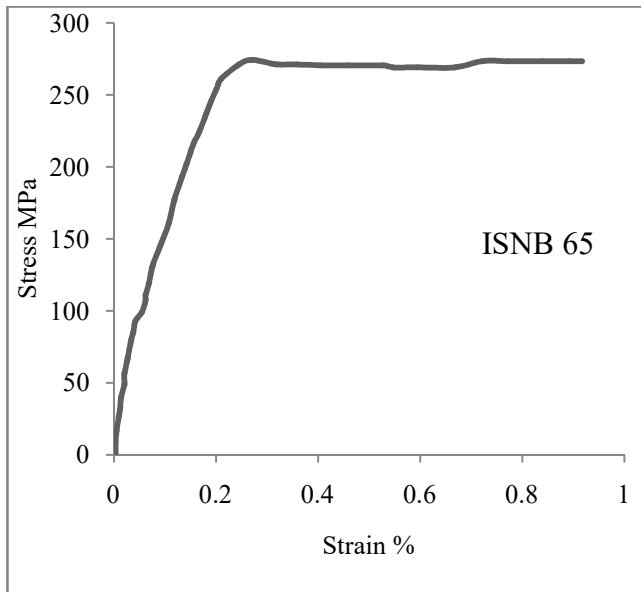


Figure 15(c): ISNB 65

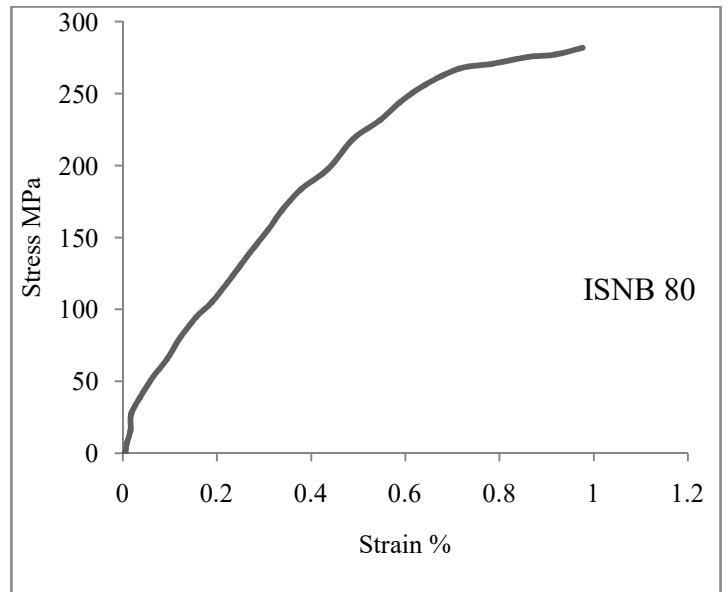


Figure 15(d): ISNB 80

Figure 15: Stress- Strain curves for four sections obtained from experiments

The material properties used in the finite element model are the average of these four curves on shown in below table. The average of these curves is taken in order to minimize the irregularities caused due to many human limitations during the forging of the material and experimental errors. Since there is not any definite yield point in the stress–strain any curve so 0.2% proof stress is taken as the yield strength of material.

Table 5: Material properties obtained from experiments

S. No.	Section	Modulus of Elasticity (E) (GPa)	Proof Stress $\sigma_{0.2\%}$ (MPa)	Ultimate Stress (σ_u) (MPa)	ϵ_f (%)
1	ISNB 40	100	300	352.12	0.75
2	ISNB 50	87.5	330	372.00	1.30
3	ISNB 65	250	255	274.13	0.95
4	ISNB 80	125	250	281.00	0.97

The buckling load values obtained from the experiments and their buckled profiles are shown below. It can be seen from the load values that as the section size increases the buckling load value also increases.

Table 6: Buckling load values of tested samples from experiments

S. NO.	Section	Compressive strength (KN) $P_{\text{Experimental}}$
1	ISNB 40	195.30
2	ISNB 50	305.31
3	ISNB 65	348.75
4	ISNB 80	434.23

Table 7: Displacement values of tested samples from experiments

S.NO.	Section	Axial displacement (mm)	Transverse displacement (mm)
1	ISNB 40	3.72	7.05
2	ISNB 50	6.71	6.86
3	ISNB 65	4.63	4.76
4	ISNB 80	4.98	3.59

Experimental displacements are reported in Table 7. It can be derived from the transverse displacements that it decreases as the cross-sectional dimensions of the circular columns increases. This happens because as the size increases the moment of inertia also increases and it provides more rigidity to the lateral deflection. Though, axial displacement does not show any such pattern. Axial displacement initially increases with the increment in the cross-sectional dimensions and then subsequently decreases with further increment in the dimensions of the cross-section of the column.

The force-displacement curves for all the four sections are shown in Figure 16. These curves show the change in the stiffness of columns as the load increases incrementally. It can be seen from curves that in the beginning, stiffness do not change much, but at a certain point, force-displacement curve becomes flat, which shows that the stiffness of the column becomes almost zero.

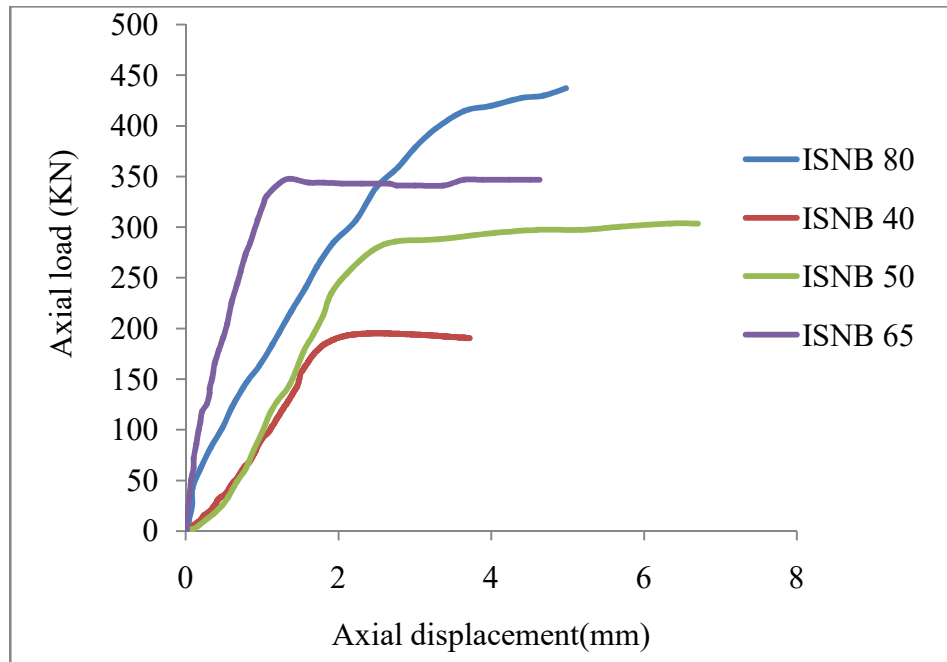


Figure 16: Force- Displacement curves

Figure 17 shows the buckling shapes of all the four sections. These buckling shapes clearly show that as the size of the section increases the curvature in shape becomes less prominent because of the increment in the moment of inertia.



Figure 17(a): ISNB 40



Figure 17(b): ISNB 50



Figure 17(c): ISNB 65



Figure 17(d): ISNB 80

Figure 17: Buckling shapes obtained from experiments

CHAPTER 5

Numerical Analysis of Tested Samples

The finite element study of samples taken under consideration for the experiment is done using the model illustrated above and the buckling load values and force-displacement curves obtained from the model compared from the experimental one in figures below. The material response curve obtained from the experiments is used to simulate these sections under compression. All the non-linearities discussed above viz. geometric nonlinearities, material nonlinearities and geometric imperfections were taken under consideration during the analysis.

Table 8: Comparison between load values obtained from experiments and proposed FE code

S.NO.	Section	Compressive strength (KN) $P_{\text{Experimental}}$	Failure mode from experiments	Compressive strength (KN) P_{FEM}	Failure mode from FEM	$\frac{P_{\text{Experimental}}}{P_{\text{FEM}}}$
1	ISNB 40	195.30	L	194.79	L	1.00262
2	ISNB 50	305.31	L	301.71	L	1.01193
3	ISNB 65	348.75	L	375.08	L	0.9298
4	ISNB 80	434.23	L	455.60	L	0.95309
Mean	-	-	-	-	-	0.97436
COV	-	-	-	-	-	0.040397

Note: 'L' represents failure mode as flexure buckling

Table 8 shows the comparison between the buckling load values for all the four sections obtained from the experiments and proposed FE code. It can be seen from these values that proposed FE code is able to predict accurate buckling load values. Here one can also compare the failure modes through experiments and one obtained from the finite element model, and can conclude that proposed finite element model is capable of accurately predicting failure modes as well.

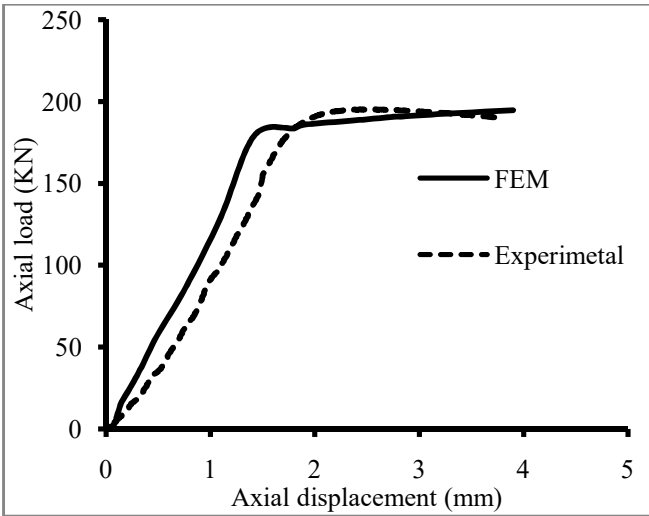


Figure 18(a): ISNB 40

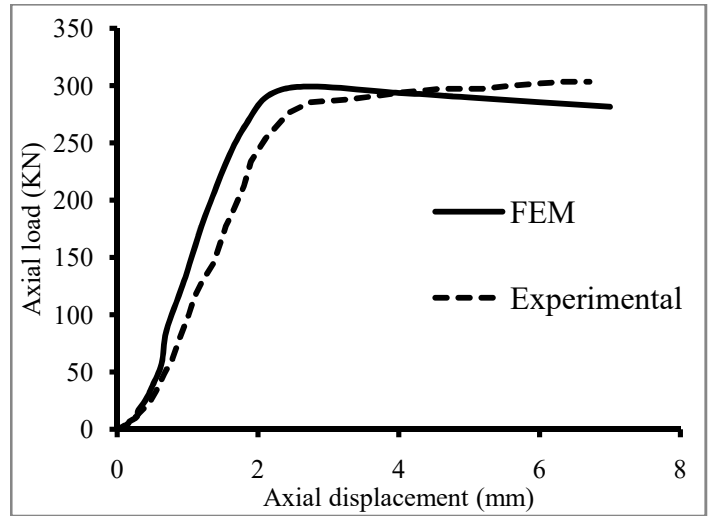


Figure 18(b): ISNB 50

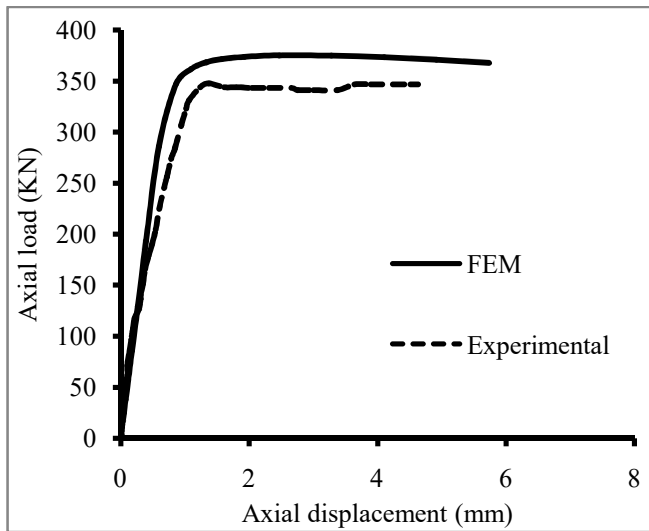


Figure 18(c): ISNB 65

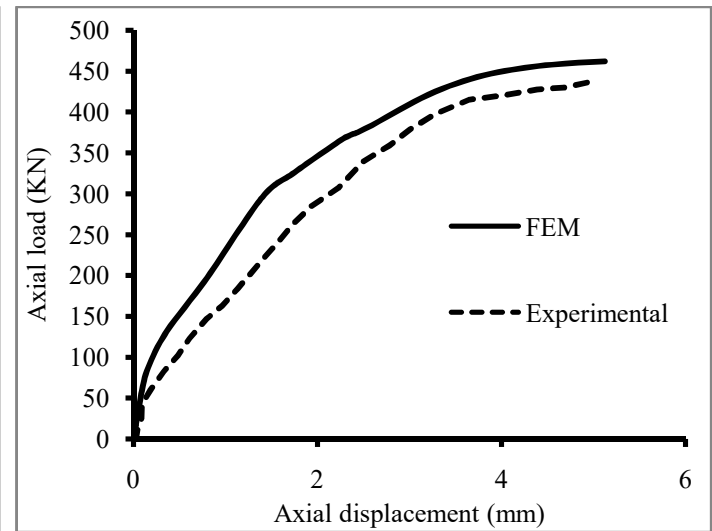


Figure 18(d): ISNB 80

Figure 18: Comparison between force displacement curves obtained from experiments and proposed FE code

Though, the proposed FE code is capable of predicting failure load values and buckling shapes accurately as can be seen in Table 8 and Figure 19. This can be attributed to the fact that the exact column profile cannot be included in the model without the help of lasers. It can be seen through Figure 18 that the proposed FE code is predicting accurate stiffness when compared with the experimental results.



Figure 19(a): ISNB 40 (Experimental)

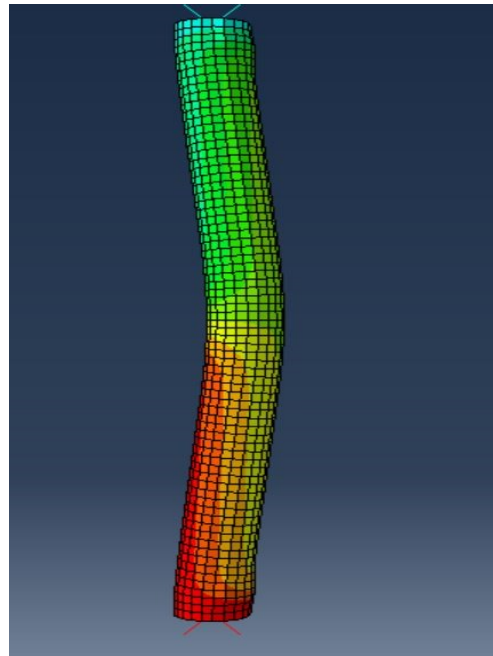


Figure 19(b): ISNB 40 (FE code)



Figure 19(c): ISNB 50 (Experimental)

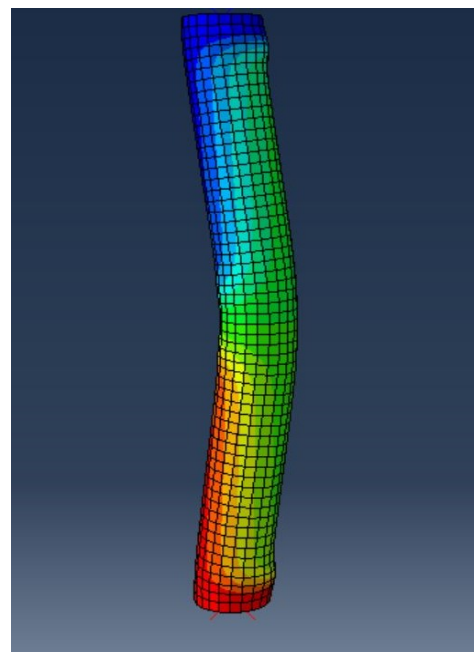


Figure 19(d): ISNB 50 (FE code)



Figure 19(e): ISNB 65 (Experimental)

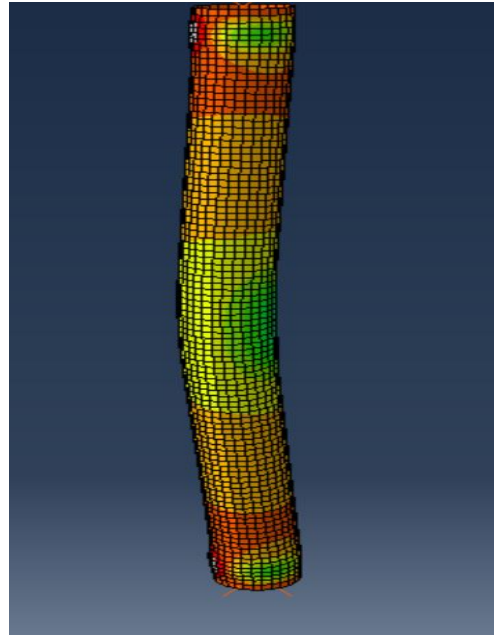


Figure 19(f): ISNB 65 (FE code)



Figure 19(g): ISNB 50 (Experimental)

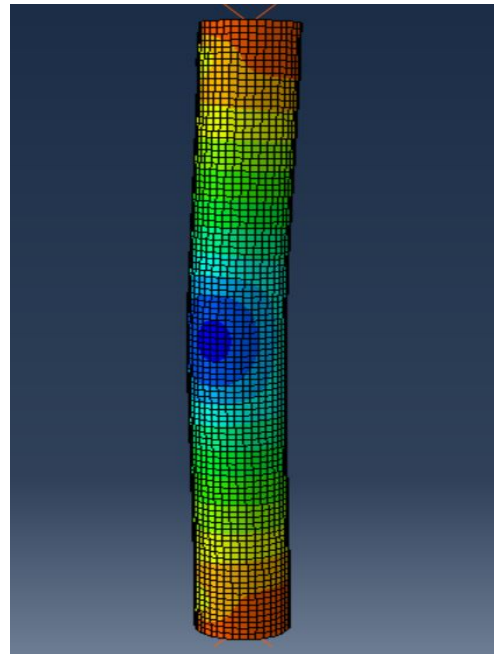


Figure 19(h): ISNB 50 (FE code)

Figure 19: Comparison of experimental buckling shape with proposed FE code

CHAPTER 6

Results and Conclusions

The validated model is applied to study the failure of circular tubes for different support conditions and lengths. Three support conditions are adopted here, namely fixed ended (BC 1), propped cantilever (BC 2) and simply supported (BC 3). Length of the columns is varied from 1.0 m to 3.0 m at a constant interval of 0.5m. Table 9, 10 and 11 contain the values of failure loads for simply supported, fixed-fixed supported and propped cantilever respectively. These tables report the mode of failure also. Here ‘L’ represents the failure through flexure buckling and ‘Y’ represents the failure through yielding of material. From the parametric studies reported in Tables 9, 10 and 11, the following conclusions can be drawn.

1. The tables reveal that for a given length and boundary condition of the axially compressed columns, the failure load increases monotonously when the diameter of the circular tubes increases and the the highest failure load is achieved for the maximum diameter of the tubular column.
2. The tables reveal that for a given length and cross-sectional dimensions of the axially compressed columns, the failure load increases monotonously when degrees of freedom decreases and the highest failure load is achieved for fixed ended condition.
3. And for same boundary conditions and cross-sectional dimensions, as the length increases the failure load value decrease. This phenomenon can be attributed to the fact that as the length increase with the same moment inertia, slenderness ratio also increased which results in lower buckling loads.
4. Failure loads obtained from proposed FE code and that from IS: 800 – 2007 are compared. One can see that IS code is continuously underestimating the failure load values as it is supposed to.
5. Figure 23 is showing the variations in buckling shapes of ISNB 65 for three different boundary conditions as length increases. It can be seen in any of the group of three shapes for same length that the most instable, in another terms most severely affected, structures under compression are the ones which have boundary conditions as simply supported. This can be justified by the fact that, for a given column, effective length is largest for simply supported and is smallest for the fixed column, and this makes fixed column a more stable column to use.
6. The comparison between the failure loads given by proposed FE code and IS: 800- 2007 is reported in the Figure 20, 21, and 22. In these figures, the dotted line parallel to x-axis represents the yield strength of the corresponding section and dotted line parallel to the y-axis represents the limiting slenderness ratio. Sections which have slenderness ratio higher than the limiting value is to be considered as a long column, and generally will fail in flexure buckling.

Table 9: Buckling loads for circular simply supported columns

S.NO.	Section	Length(mm)	Failure load (kN) from FEM	Failure load (kN) from IS code	Failure Mode
1	ISNB 40	1000	120.76	95.821	L
2	ISNB 65	1000	264.54	193.072	L
3	ISNB 80	1000	403.59	255.7544	L
4	ISNB 90	1000	515.95	297.682	Y
5	ISNB 100	1000	720.39	380.061	Y
6	ISNB 110	1000	805.67	454.278	Y
7	ISNB 125	1000	970.31	504.284	Y
8	ISNB 135	1000	1090.34	554.257	Y
9	ISNB 40	1500	109.88	70.961	L
10	ISNB 65	1500	242.56	177.562	L
11	ISNB 80	1500	360.25	240.966	L
12	ISNB 90	1500	469.42	284.306	L
13	ISNB 100	1500	520.37	365.937	Y
14	ISNB 110	1500	710.11	439.857	Y
15	ISNB 125	1500	880.66	490.292	Y
16	ISNB 135	1500	930.72	540.562	Y
17	ISNB 40	2000	69.14	46.893	L
18	ISNB 65	2000	213.45	153.428	L
19	ISNB 80	2000	321.29	219.527	L
20	ISNB 90	2000	411.76	266.387	L
21	ISNB 100	2000	543.72	348.172	L
22	ISNB 110	2000	631.88	422.576	Y
23	ISNB 125	2000	770.90	474.166	Y
24	ISNB 135	2000	811.22	525.228	Y
25	ISNB 40	2500	44.95	31.867	L
26	ISNB 65	2500	187.24	122.628	L
27	ISNB 80	2500	229.33	189.167	L
28	ISNB 90	2500	359.95	241.241	L
29	ISNB 100	2500	441.29	324.291	L
30	ISNB 110	2500	561.71	400.444	L
31	ISNB 125	2500	650.65	454.366	Y
32	ISNB 135	2500	720.21	507.067	Y
33	ISNB 40	3000	31.44	22.814	L
34	ISNB 65	3000	130.97	94.589	L
35	ISNB 80	3000	180.11	154.605	L
36	ISNB 90	3000	256.87	208.758	L
37	ISNB 100	3000	320.44	291.06	L
38	ISNB 110	3000	370.44	371.316	L
39	ISNB 125	3000	453.87	429.11	L
40	ISNB 135	3000	572.33	484.627	L

Table 10: Buckling loads for circular fixed columns

S.NO.	Section	Length(mm)	Failure load (kN) from FEM	Failure load (kN) from IS code	Failure Mode
1	ISNB 40	1000	198.76	106.139	L
2	ISNB 65	1000	296.05	200.981	L
3	ISNB 80	1000	493.52	264.022	Y
4	ISNB 90	1000	545.79	305.668	Y
5	ISNB 100	1000	770.83	388.85	Y
6	ISNB 110	1000	904.72	463.529	Y
7	ISNB 125	1000	1007.82	513.458	Y
8	ISNB 135	1000	1184.73	563.376	Y
9	ISNB 40	1500	167.27	96.745	L
10	ISNB 65	1500	289.26	193.688	L
11	ISNB 80	1500	407.83	256.377	Y
12	ISNB 90	1500	487.55	298.276	Y
13	ISNB 100	1500	584.71	380.71	L
14	ISNB 110	1500	792.91	454.96	Y
15	ISNB 125	1500	897.90	504.944	Y
16	ISNB 135	1500	1002.35	554.917	Y
17	ISNB 40	2000	138.67	81.994	L
18	ISNB 65	2000	288.59	184.591	L
19	ISNB 80	2000	390.53	247.467	L
20	ISNB 90	2000	448.67	290.048	Y
21	ISNB 100	2000	611.47	371.899	Y
22	ISNB 110	2000	697.31	445.874	L
23	ISNB 125	2000	785.78	496.078	Y
24	ISNB 135	2000	853.67	546.183	Y
25	ISNB 40	2500	124.16	64.141	L
26	ISNB 65	2500	287.45	172.458	L
27	ISNB 80	2500	306.78	236.379	L
28	ISNB 90	2500	415.76	280.357	L
29	ISNB 100	2500	498.12	361.922	L
30	ISNB 110	2500	617.47	435.875	Y
31	ISNB 125	2500	713.10	486.519	Y
32	ISNB 135	2500	791.14	536.932	Y
33	ISNB 40	3000	116.15	48.873	L
34	ISNB 65	3000	236.89	156.266	L
35	ISNB 80	3000	282.98	222.068	L
36	ISNB 90	3000	340.54	268.466	L
37	ISNB 100	3000	387.85	350.174	L
38	ISNB 110	3000	411.30	424.49	L
39	ISNB 125	3000	597.45	475.915	L
40	ISNB 135	3000	620.37	526.867	L

Table 11: Buckling loads for circular propped cantilever columns

S.NO.	Section	Length(mm)	Failure load (kN) from FEM	Failure load (kN) from IS code	Failure Mode
1	ISNB 40	1000	150.56	102.344	L
2	ISNB 65	1000	289.88	197.769	L
3	ISNB 80	1000	457.23	260.601	L
4	ISNB 90	1000	521.48	302.324	L
5	ISNB 100	1000	745.71	385.154	Y
6	ISNB 110	1000	860.78	459.613	Y
7	ISNB 125	1000	983.94	509.553	Y
8	ISNB 135	1000	1121.97	559.493	Y
9	ISNB 40	1500	148.40	87.12	L
10	ISNB 65	1500	272.41	187.649	L
11	ISNB 80	1500	380.57	250.393	L
12	ISNB 90	1500	479.31	292.71	L
13	ISNB 100	1500	557.43	374.715	L
14	ISNB 110	1500	750.47	448.745	Y
15	ISNB 125	1500	887.83	498.861	Y
16	ISNB 135	1500	967.90	548.911	Y
17	ISNB 40	2000	126.64	65.483	L
18	ISNB 65	2000	243.87	173.525	L
19	ISNB 80	2000	350.12	237.336	L
20	ISNB 90	2000	430.89	281.171	L
21	ISNB 100	2000	570.77	362.747	L
22	ISNB 110	2000	665.75	436.689	L
23	ISNB 125	2000	773.87	487.289	Y
24	ISNB 135	2000	822.78	537.669	Y
25	ISNB 40	2500	103.65	46.893	L
26	ISNB 65	2500	221.82	153.428	L
27	ISNB 80	2500	254.09	219.527	L
28	ISNB 90	2500	389.99	266.387	L
29	ISNB 100	2500	474.33	348.172	L
30	ISNB 110	2500	594.29	422.576	L
31	ISNB 125	2500	685.36	474.166	L
32	ISNB 135	2500	743.44	525.228	Y
33	ISNB 40	3000	63.80	34.287	L
34	ISNB 65	3000	204.56	128.843	L
35	ISNB 80	3000	221.32	195.855	L
36	ISNB 90	3000	310.53	246.928	L
37	ISNB 100	3000	351.57	329.67	L
38	ISNB 110	3000	396.72	405.361	L
39	ISNB 125	3000	536.12	458.711	L
40	ISNB 135	3000	594.57	510.994	L

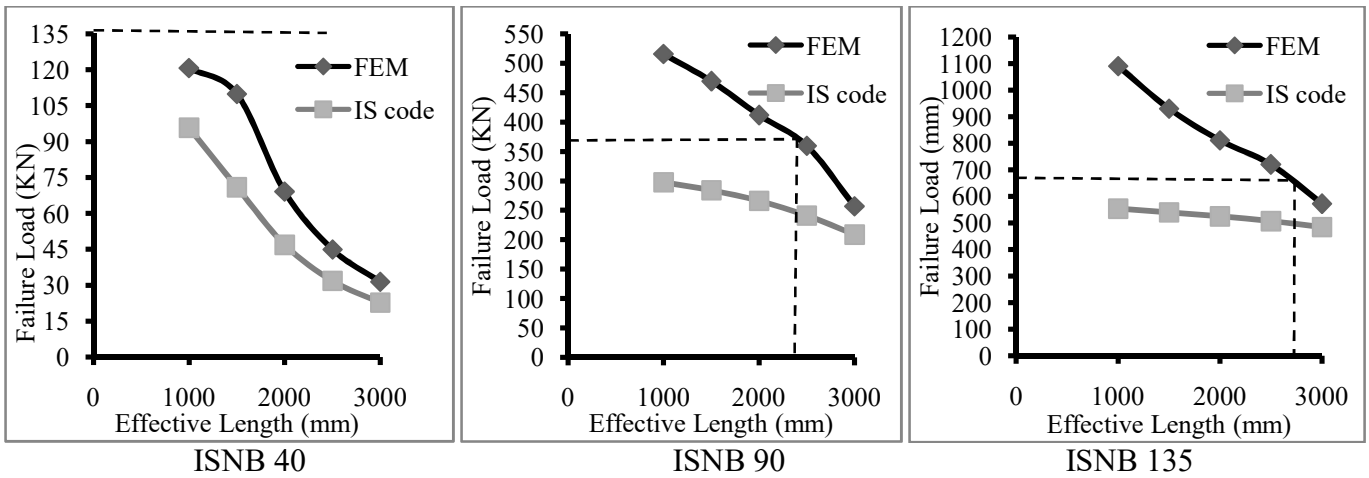


Figure 20: Comparison of Failure load vs. Effective length between values obtained from FE code and IS code for Simply Supported

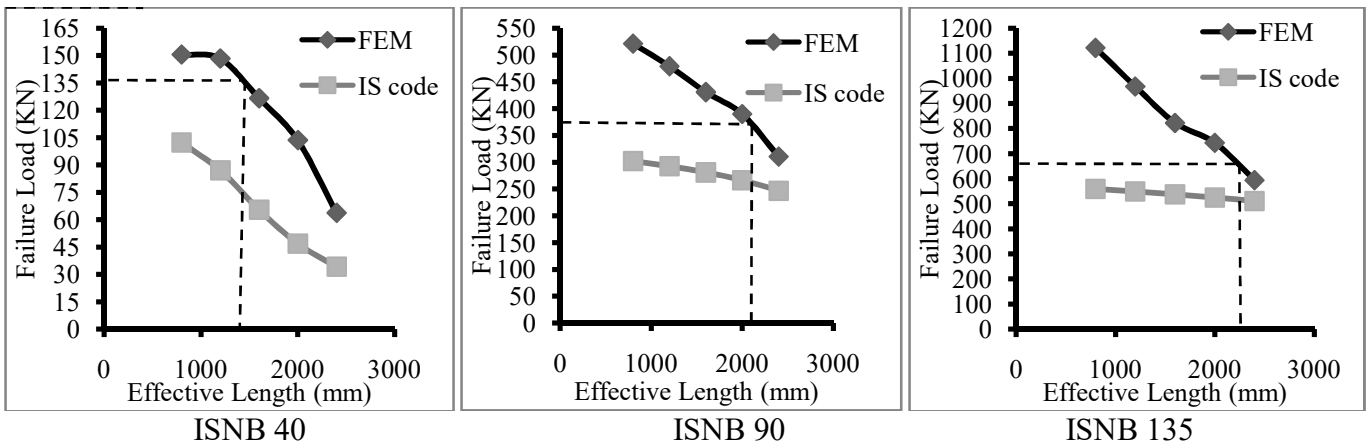


Figure 21: Comparison of Failure load vs. Effective length between values obtained from FE code and IS code for Propped cantilever Supported

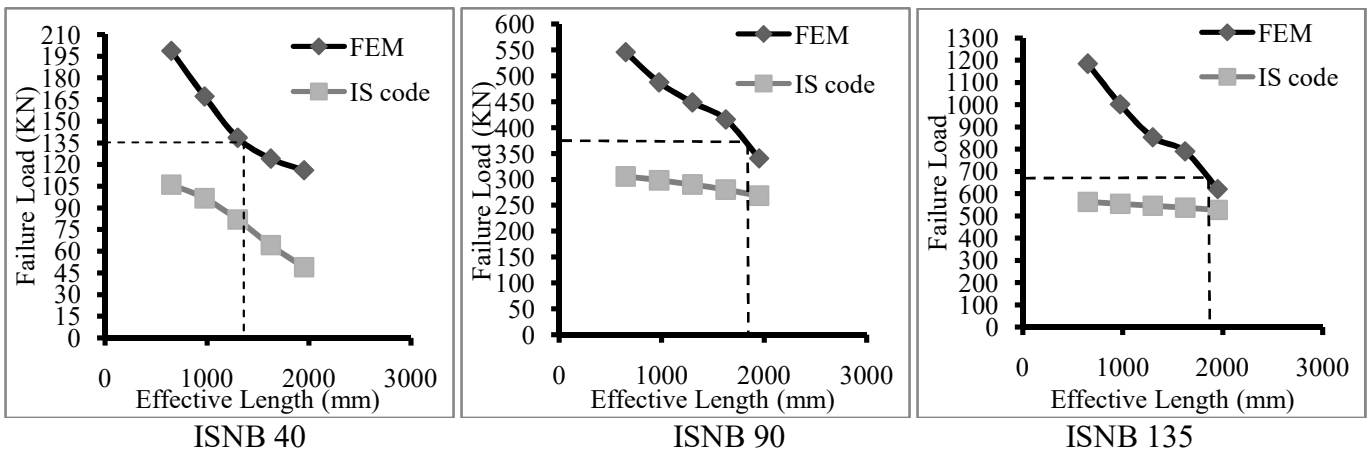


Figure 22: Comparison of Failure load vs. Effective length between values obtained from FE code and IS code for Fixed Supported

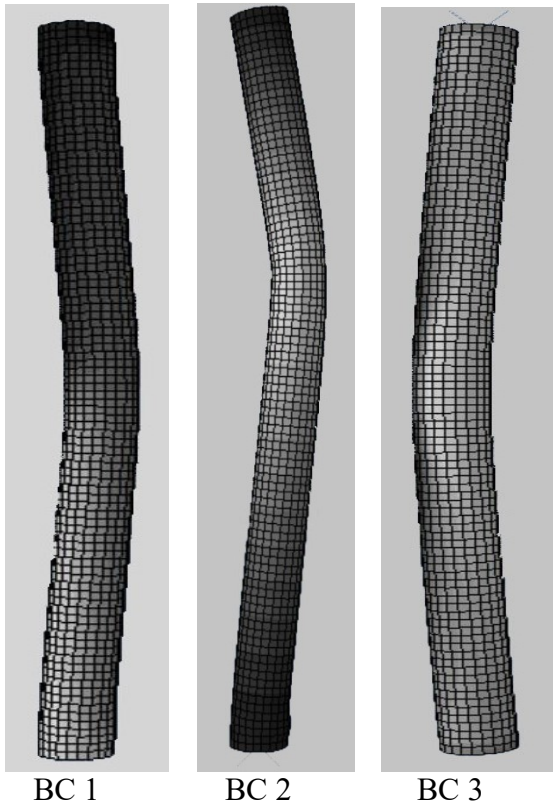


Figure 23(a): Length 1000

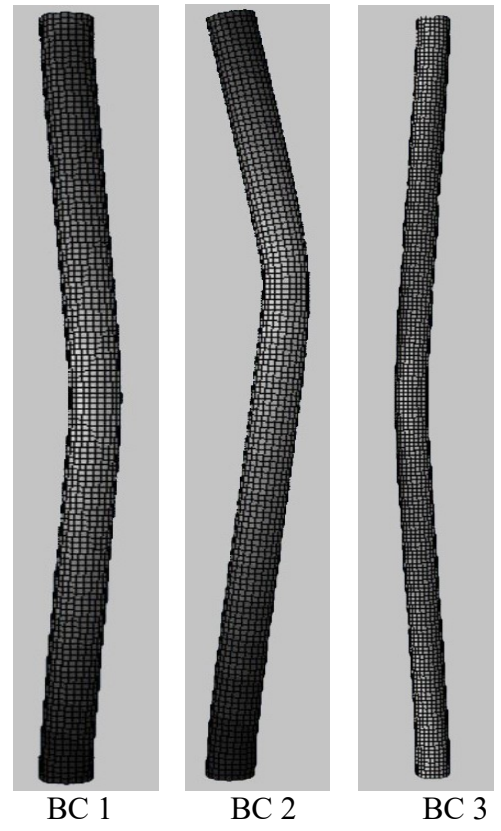


Figure 23(b): Length 1500

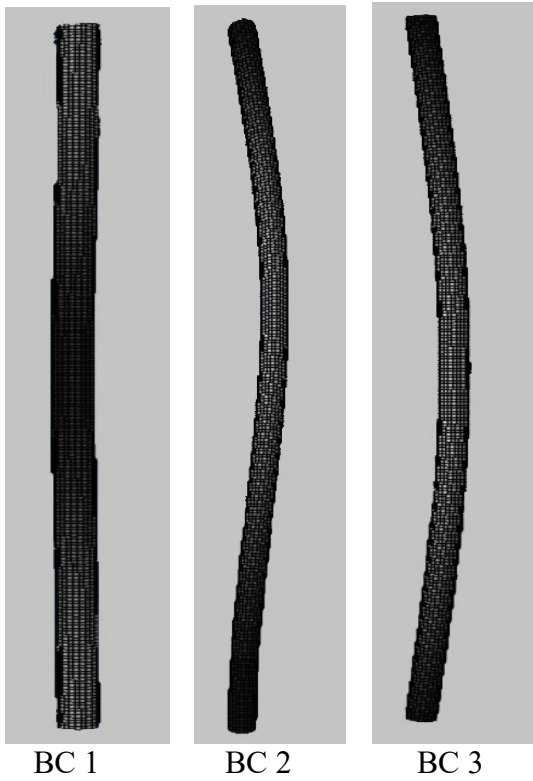


Figure 23(c): Length 2500

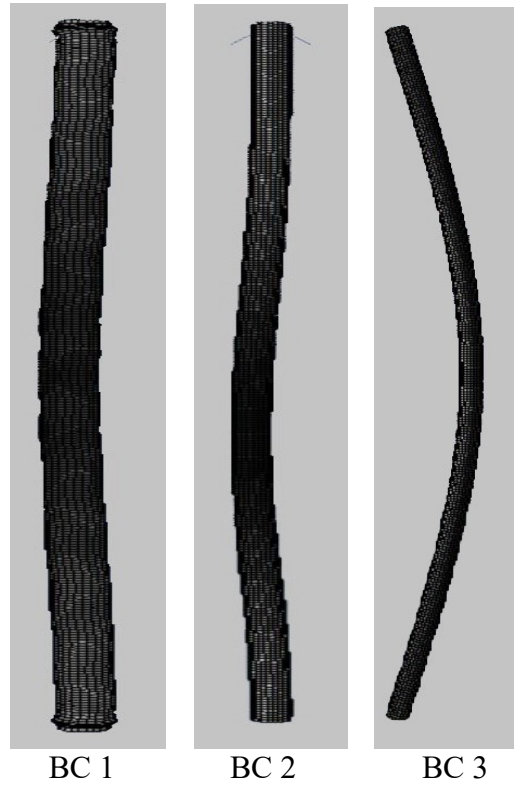


Figure 23(d): Length 3000

Figure 23: Buckling shapes of ISNB 65 for three different boundary condition and for four different lengths

CHAPTER 7

Future Scope of Work

In future, this study can be extended to develop the finite element model to simulate the behavior and to predict failure load of various types of hollow sections which are being used currently in construction projects. Some of them are as follows.

- Stiffened square hollow section
- Stiffened rectangular hollow section
- Stiffened circular hollow section
- Battened Columns

Some of these sections are already been studied by other researchers but they have followed the American, European and Australian/ New Zealand code of practices [2], [5]. There is no study available currently in literature based on Indian codes of practices, so these sections can be further studied to fill the lacuna.

References

1. Ellobody, Ehab, and Ben Young, "Structural performance of cold-formed high strength stainless steel columns" ,*Journal of Constructional Steel Research* ,**61**, pp.1631-1649 ,2005.
2. Ellobody, Ehab,"Buckling analysis of high strength stainless steel stiffened and unstiffened slender hollow section columns", *Journal of Constructional Steel Research* ,**63**, pp.145-155 ,2007.
3. ABAQUS (2017), "ABAQUS Documentation", *Dassault Systèmes, Providence, RI, USA*.
4. Young, Ben, and Kim JR Rasmussen,"Tests of fixed-ended plain channel columns" ,*Journal of Structural Engineering*,**124**, pp.131-139 ,1998.
5. Dabaon, Mohamed, Ehab Ellobody, and Khaled Ramzy, "Nonlinear behaviour of built-up cold-formed steel section battened columns" ,*Journal of Constructional Steel Research*,**110**, pp.16-28 ,2015.
6. Origin (Pro), Version 2019b, *OriginLab Corporation*, Northampton, MA, USA.
7. Zhao, Ou, Leroy Gardner, and Ben Young, "Structural performance of stainless steel circular hollow sections under combined axial load and bending–Part 1: Experiments and numerical modelling" ,*Thin-Walled Structures* ,**101**,pp.231-239 ,2016.
8. Young, Ben, and Jintang Yan, "Channel columns undergoing local, distortional, and overall buckling" ,*Journal of Structural Engineering* , ,ASCE,**128**,pp.728-736, 2002.
9. Theofanous, M., T. M. Chan, and L. Gardner, "Structural response of stainless steel oval hollow section compression members", *Engineering Structures* ,**31**,pp.922-934, 2009.
10. Gardner, L., and D. A. Nethercot, "Numerical modeling of stainless steel structural components—a consistent approach" , *Journal of Structural Engineering*, ASCE,**130**,pp.1586-1601, 2004.
11. Afshan, S., and L. Gardner, "Experimental study of cold-formed ferritic stainless steel hollow sections", *Journal of Structural Engineering*, ,ASCE,**139**,pp.717-728, 2013.
12. Gupta, P. K., Ziyad A. Khaudhair, and A. K. Ahuja, "A study on load carrying capacity and behaviour of concrete filled steel tubular members subjected to axial compression", In *the 11th International Conference on Concrete Engineering and Technology 2012*, pp. 337-342, 2012.
13. Barbero, Ever, and John Tomblin, "Euler buckling of thin-walled composite columns", *Thin-walled structures*, **17**,pp. 237-258, 1993.
14. Liu, Y., and B. Young, "Buckling of stainless steel square hollow section compression members", *Journal of Constructional Steel Research*, **59**, pp.165-177 ,2003.
15. Zhu, Ji-Hua, and Ben Young, "Numerical investigation and design of aluminum alloy circular hollow section columns", *Thin-Walled Structures*, **46**,pp.1437-1449 ,2008.